Mechanical and Dimensional Stability of Gelatin-Based Hydrogels through 3D Printing-Facilitated Confined Space Assembly

Heng Li Chee[1], Yashaaswini M[2], Jaedeok Kim[3], Jing Wen Koo[3], Ping Luo[1], Faris H. Ramli[3,4], Jennifer L. Young[3,4], FuKe Wang[1,*]

[1]Institute of Materials Research and Engineering, Agency for Science, Technology and Research, 2 Fusionopolis Way, Innovis #08-03, Singapore 138634

[2]School of Materials Science and Engineering, Nanyang Technological University (NTU) , 50 Nanyang Avenue, Singapore 639798

[3]Mechanobiology Institute (MBI), National University of Singapore (NUS), 5A Engineering Drive 1, Singapore 117411

[4]Department of Biomedical Engineering, College of Design and Engineering, National University of Singapore (NUS), 4 Engineering Drive 3, Singapore 117583

* Correspondence and requests for materials should be addressed to WFK (email: wangf@imre.a-star.edu.sg)

Abstract

Hydrogels have emerged as promising biomaterials for tissue regeneration, yet their inherent swelling can cause deformation and reduced mechanical properties, posing challenges for practical applications in biomedical engineering. Traditional methods to reduce hydrogel swelling often involve complex synthesis procedures with limited flexibility. Inspired by nature's efficient designs, we present here the approach to improve hydrogel performance using 3D printing-assisted microstructure engineering. By utilizing polymerization-induced phase separation of hydrogel from co-polymerization of Gelatin methacrylate and hydroxyethyl methacrylate (poly(GelMA-*co*-HEMA)) in the confined space during vat photopolymerization (VPP) 3D printing, we replicate the cuttlebone-like microstructure of hydrogels with enhanced mechanical properties and swelling resistance. We demonstrate here a four-fold increase in elastic modulus compared to bulk polymerization of poly(GelMA-*co*-HEMA), together with improved mechanical and dimensional stability. This method offers promising opportunities for practical biomedical and tissue engineering applications, overcoming previous limitations in hydrogel design and performance.

Keywords: Bioinspired; tough hydrogels, anti-swelling; cuttlebone, polymerization-induced phase separation, 3D printing

Introduction

High-performance biomaterials are becoming increasing popular for their use in innovative designs and tissue regeneration. While various synthetic and natural biomaterials have been developed, their biocompatibility and functionality still present challenges for biomedical applications.[1, 2] Hydrogels, with their ability to promote cell proliferation, migration, and differentiation through specific cell-material interactions, has become the most preferred biomaterials for tissue regeneration.[3-5] The high water content, porosity, and similarity to natural extracellular matrix (ECM) make hydrogels particularly suitable for biomedical studies.[6] However, their intrinsic hydrophilic and porous network often leads to unavoidable swelling in aqueous media, significantly compromising their physical performance, especially in terms of mechanical strength, dimensional stability, and cellular adhesion.[7-9] This limitation severely hampers their use in tissue engineering, regenerative medicine, implant electronics, and artificial tissues.[10-13] To address these issues, recent efforts have focused on reducing the swelling behavior of hydrogels. The most popular strategy involves increasing the crosslinking density of hydrogels through either covalent or physical cross-linking.[14-25] Other approaches include regulating the balance of hydrophobic-hydrophilic or post-treatment.[26-28] While these approaches have proven effective in achieving desirable anti-swelling properties and mechanical performance, they require sophisticated design, complex synthesis, and time-consuming processes. Furthermore, they often lack the flexibility to adjust the hydrogel's performance due to pre-set functionalities and chemistries.[7, 25, 29, 30]

In contrast, creatures in nature have evolved unique microstructures with impressive mechanical performance and stability, utilizing intrinsic weak materials that are widely available in their surroundings.[31] For example, nacre, found in the shells of mollusks, exhibits superior toughness through its aligned microstructures,[32, 33] while cuttlefish bones are ultra-

lightweight and damage-resistant through their multiple layered chambers, providing control of movement even at great depth, *e.g.* 600 meters below sea level.[34, 35]

In this work, we demonstrate the substantially improved mechanical properties, heightened swelling resistance, and enhanced mechanical stability of poly(GelMA-*co*-HEMA) hydrogels by 3D printing-assisted microstructure engineering. By utilizing polymerization-induced phase separation in the confined space during vat photopolymerization (VPP) 3D printing of poly(GelMA-*co*-HEMA), we achieve high-performance hydrogels with a uniform cuttlebone-like microstructure. The 3D printing process, which mimics the natural creation of intricate multilayer materials as observed in *e.g.* mollusk shells, involves layer-by-layer construction.[36-38] In VPP-based 3D printing methods such as Digital Light Processing (DLP) and Liquid Crystal Display (LCD) printing, the printing platform gradually lowers into the resin based on the desired layer thickness (**LT**), creating a confined space between the platform and tray (see Figure 1). When exposed to UV light, the ink undergoes photopolymerization-induced phase separation, causing polymer chains to condense within the confined space.[39, 40] The polymer-rich domains then form the walls of pores within the hydrogel, ultimately creating a layered, cuttlefish bone-like microstructure. Further increasing the **LT** diminished the confining effect, reverting the microstructure of the hydrogel to a random porous arrangement same as bulk polymerization. Due to the uniform cuttlefish bone-like microstructure and condensed polymeric walls, we observe a four-fold increase in the elastic modulus of 3D-printed hydrogels of poly(GelMA-co-HEMA) compared to those fabricated via bulk polymerization. Most importantly, the printed structures exhibit significantly enhanced swelling resistance and mechanical stability, rendering our approach promising for practical applications in biomedical and tissue engineering.

Results and Discussion

Cuttlefish Bone-Like Microstretches of 3D Printed Poly(GelMA-*co*-HEMA) Hydrogels.

Gelatin, a form of denatured collagen, has gained popularity in the field of tissue engineering due to its ability to provide cell adhesion recognition motifs for cell-substrate interaction.[41, 42] Meanwhile, poly(hydroxyethyl)methacrylate (pHEMA), made from methacrylate monomers, is a biocompatible synthetic polymer that can be used for various soft tissue regenerative applications because of its ability to introduce mesoscopic pores and good mechanical characteristics.[43, 44] By sequential crosslinking of methacrylate modified Gelatin (GelMA) with polyHEMA, an interpenetrating network of pHEMA and GelMA has been reported.[45] In this study, we utilize a LCD 3D printer to print poly(GelMA-co-HEMA) hydrogel with varying ratio of GelMA and HEMA, which were cross-linked covalently. For example, hydrogels printed from a combination of 5% GelMA and 25% HEMA are labeled as G5H25-3D, while hydrogels printed from combination of 10% GelMA and 20% HEMA are labeled as G10H20-3D. To understand the impact of material architecture over composition, hydrogels with the same formulations as 3D printed samples were also prepared using bulk polymerization and labeled as G5H25-B and G10H20-B, respectively.

Figure 1a shows the 3D printing process of G10H20 on an LCD printer, which creates 3D objects layer by layer by using UV light to selectively cure liquid resin in the tray. The platform is raised after each layer is cured, with a 50 μm layer thickness being used in this case. The printing ink, which consists of water, GelMA, and HEMA, will then flow into the confined space for the next layer. Free radicals are generated and polymerization is initiated when patterned light projects into the confined space. During the printing process, photopolymerization-induced phase separation causes the polymer chains to condense into polymer-rich domains, contributing to the formation of a 3D porous network.[39, 44, 46] These condensed polymer domains are expected to adhere to both the previously formed polymer

layer and the fluorinated ethylene propylene (FEP) film of the tray,[47-49] resulting in an evenly distributed 'wall-septa' structure, as shown in Figure 1a. The repeated printing process results in multiple layered-cellular microstructures, similar to those found in cuttlebones (Figure 1b).

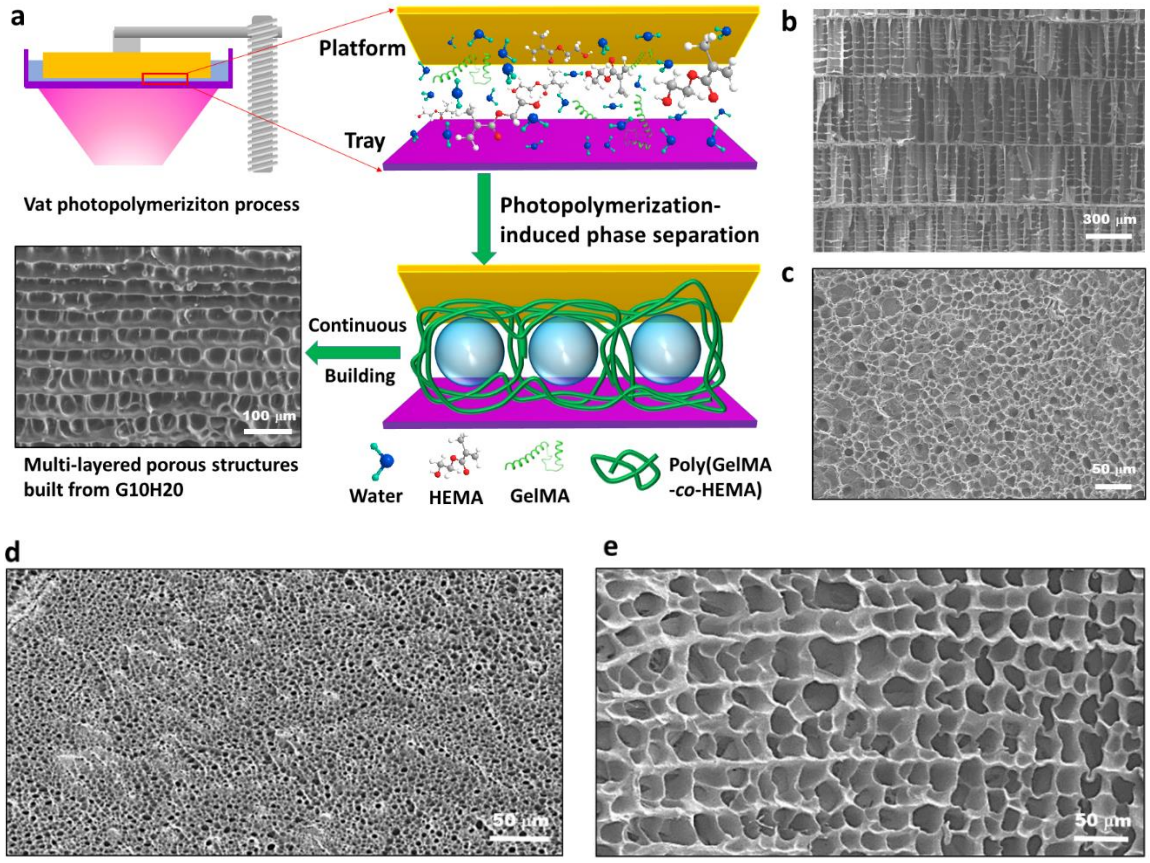

Figure 1. (a) Schematic demonstration the process of 3D printing of G10H20 using a LCD 3D printer and the formation of the cuttlefish bone-like microstructures. Cross-sectional SEM image of (b) the cuttlefish bone, (c) G10H20 hydrogel prepared through bulk polymerization, (d) G5H25 hydrogel that was prepared through bulk polymerization and (e) G5H25 hydrogel that was prepared through 3D printing.

On the other hand, hydrogels prepared through bulk polymerization exhibit a typical random porous structure with relatively thin pore walls, as seen in Figure 1c. The differences in architecture for 3D printed vs. bulk polymerization can be observed for multiple hydrogel compositions (as illustrated in Figure 1d and 1e for G5H25). Specifically, hydrogels produced through bulk polymerization showed pronounced differences in pore size that were dependent on the composition, while hydrogels produced through 3D printing displayed less

sensitivity to composition. As shown in Figure 1c and 1d, G10H20 and G5H25 produced through bulk polymerization displayed the maximum distributed pore size of ~ 5 and 15 μm, respectively. However, both hydrogels produced through 3D printing had a maximum pore size of ~25 μm when they were printed with a layer thickness of 50 μm (Figure S1). The significant differences in pore size and arrangement between hydrogels produced through different methods suggest that the pores in the hydrogels produced through 3D printing are more strongly influenced by the fabrication process and the confined space during printing.

To verify the confined space effect, the printing layer thickness was set to 200, 300 and 400 μm in the printing files with other factors remained unchanged. Figure 2 demonstrates the significant impact of printing layer spacing on the pore size of both hydrogels, G5H25 and G10H20. When the printing layer spacing changes from 50 μm to 200 and 300 μm, the pore size of G5H25 increases from 25 μm to 198 and 280 μm, respectively. A similar trend was observed in G10H20, where the pore size shifted from 25 μm to 180 and 250 μm, respectively, as the layer spacing changed from 50 μm to 200 and 300 μm. It can thus be concluded that the pore size is mainly controlled by the confinement effect of the layer spacing. It is important to note that the layer thickness observed in the SEM images is smaller than the set layer thickness, due to sample shrinkage during SEM sample preparation via freeze-drying (Figure S2). As a result, the actual pore sizes are larger than those measured in the SEM analysis. To confirm this, the as-printed wet hydrogel was cross-sectioned and measured under an optical microscope, as shown in Figure S3. The optical microscopic images showed much more consistent layer thicknesses with the set printing thickness and revealed larger pore sizes as compared to those observed in the SEM analysis (Figure 2). When increasing the printing layer thickness to 400 μm, the confinement effect has a reduced impact on the hydrogel structure. The microstructure of the printed hydrogels reverts to that

of a randomly porous structure, similar to those formed through bulk polymerization, but with larger pore sizes.

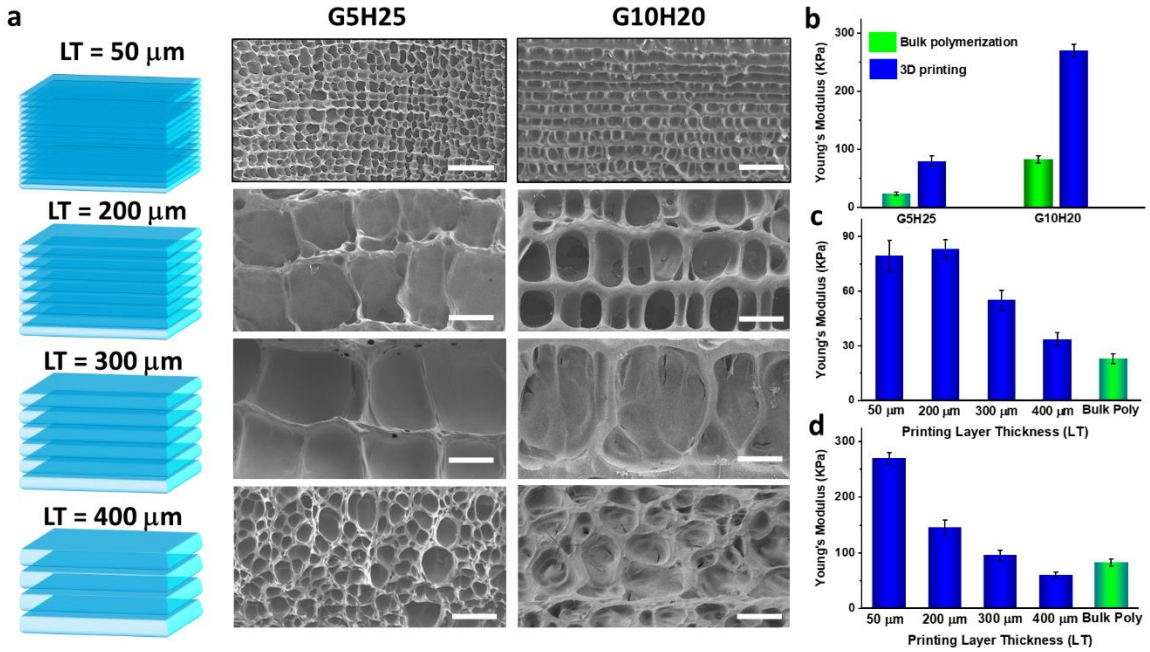

Figure 2. (a) Diagram of the layer thickness (**LT)** setting and cross-sectional SEM images of G5H25-3D and G10H20-3D hydrogels printed at a programmed **LT** of 50µm, 200µm 300µm and 400µm. Comparison of Young's modulus of (b) G5H25 and G10H20 hydrogels fabricated through 3D printing and bulk polymerization, (c) G5H25-B and G5H25-3D hydrogels printed with different **LT** of 50µm, 200µm 300µm and 400µm and (d) G10H20-B and G10H20-3D hydrogels printed with different **LT** of 50µm, 200µm 300µm and 400µm. Scale bar: 100 µm.

Besides printing layer thickness, the ink composition also influences the confined space assembly and thus the printed microstructures. When further reducing HEMA monomer content in the component (e.g., G15H15 or G20H10), cross-sectional SEM images show diminished confined space effects (Figure S4). Decreasing HEMA monomer content leads to diminished polymerization-induced phase separation and tends to promote the formation of homogeneous hydrogel structures. This may be ascribed to the content of HEMA in influencing phase separation. Water acts as a good solvent for HEMA monomers but is a poor solvent for polyHEMA, as documented in the literature[50-52] and our previous work.[44] Polymerization-induced phase separation occurs when the content of the HEMA is higher

enough in the ink.[53, 54] Further reducing the HEMA content decrease the ratio of the hydrophobic moiety and shortens the PHEMA polymer chain, thereby restricting phase separation. The low content of the hydrophobic segment precludes phase separation, leading to the inability to achieve uniform microstructures, as evidenced in hydrogels G5H25 and G10H20. This can also be observed from the increase in opacity of the 3D printed G5H25 compared to G10H20, which suggests a higher degree of phase separation in the printed G10H20. This observation indicates the formation of an immiscible aqueous phase within the 3D printed hydrogels while all the bulky polymerized hydrogel are transparent in water.[55, 56] Polymerization-induced phase separation facilitates the formation of polymer-rich domains where the polymer chains are poorly hydrated.[39] This enhances hydrogen bonding and entanglement between polymer chains, resulting in a stronger layered-cellular microstructure, as shown in Figures 1 and 2.

Enhanced Hydrogel Performance by 3D Printing Process. The elastic modulus of hydrogels is known to influence cellular fate and function; thus, we sought to understand how confined space assembly and composition influence mechanical properties of our materials. Figure 2b compares the elastic modulus of hydrogels fabricated through 3D printing and bulk polymerization. We observed that an increase in the GelMA content leads to an increase in the elastic modulus of the hydrogel, as GelMA itself is known to result in a rigid structure upon polymerization. Interestingly, in contrast to previous studies, the results showed that the 3D printed hydrogels displayed a nearly 400% increase in modulus compared to hydrogels prepared through bulk polymerization. Typically, hydrogels fabricated through 3D printing processes exhibit poor mechanical properties due to the weak interaction between building layers, limiting their use in practical applications.[57] As discussed above, the increased modulus of the 3D-printed hydrogels is attributed to polymerization-induced phase separation, which leads to the condensation of polymer chains and enhances hydrogen

bonding and chain entanglement. As shown in Figure 2a, the 3D-printed hydrogels exhibit thicker polymerized walls and well-organized pores, resulting from the polymer chain condensation, which likely contributes to the improved modulus.

The enhancement mechanism achieved through confined assembly was further explored through mechanical testing of G5H25-3D and G10H20-3D samples with varying pore sizes achieved through programmed printing layer thickness, as depicted in Figure 2c and 2d. The results showed a decrease in the modulus as the pore size increased. Notably, the samples with the smallest printing layer thickness (50 μm) exhibited the highest modulus for both G5H25 and G10H20. We believe the mechanical enhancement also arises from the microstructure engineering of the printed hydrogel, which mimics the structure of cuttlebone. Cuttlebone, composed mainly of brittle aragonite, demonstrates remarkable mechanical properties due to its intricate wall-septa microstructure, resulting in high specific stiffness (8.4 MN.m/kg) and significant energy absorption (4.4 KJ/kg) upon loading.[35] The mechanical enhancement induced by this microstructure has been validated through molecular dynamics (MD) simulations[35, 58, 59] and has been demonstrated in various engineered materials such as ceramics, metals, and polymers.[60-62] Therefore, we propose that the outstanding performance of the hydrogel is largely attributed to its lamellar septa microstructure and phase separation-induced polymer chains condensation, showing significant improvements compared to hydrogels with random porous structures.

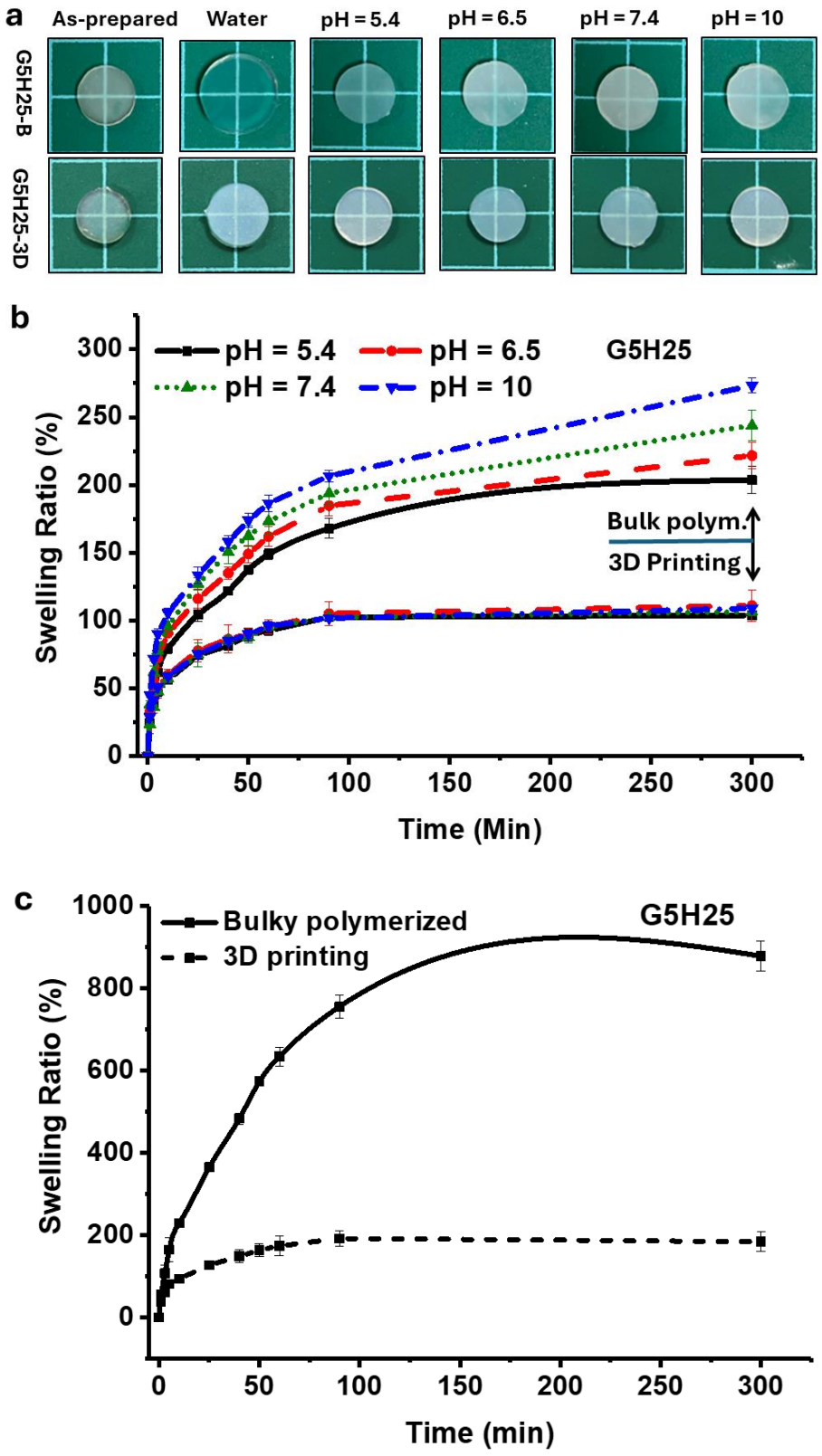

Figure 3. (a) Visual representation of as-prepared G5H25-B and G5H25-3D hydrogels and after 180 minutes of swelling in de-ionized (DI) water and phosphate-buffered saline (PBS) of varying pHs (5.4, 6.5, 7.4, 10). Swelling ratio of hydrogel G5H25 over a period of 10, 20, 30, 60, 90, 300 minutes in (b) PBS of varying pHs (5.4, 6.5, 7.4, 10) and in (c) DI water. Scale bar: 1.5mm.

Swelling Kinetic in Various Media. The uniform microstructures of 3D-printed hydrogels contribute to their improved anti-swelling properties, making them ideal for biomedical applications where swelling is undesirable. Previous studies have highlighted that hydrogels based on polyHEMA and gelatin tend to absorb water, resulting in noticeable swelling and diminished mechanical properties in aqueous environments.[7] However, the condensed polymer chains and formation of cuttlebone-like microstructures in 3D-printed poly(GelMA-*co*-HEMA) hydrogels restricts this swelling behavior. For instance, as illustrated in Figure 3a, the 3D-printed G5H25 hydrogel exhibited significantly reduced swelling when immersed in phosphate-buffered saline (PBS) at various pH levels compared to its bulk-polymerized counterpart. Notably, both the 3D-printed and bulk-polymerized hydrogels have similar water content and gel fraction, as indicated in Figure S6, with values of 62 ± 3% and 97 ± 2%, respectively.

Figures 3b and 3c present the comparison of the swelling behavior between hydrogels fabricated via bulk polymerization and 3D printing, assessing their mass changes from freeze-dried to gel states in various media. In Figure 3b, hydrogel G5H25, synthesized through 3D printing, exhibited non-swelling in PBS buffer solutions (~100%) across all tested pH conditions, while the bulk polymerized counterpart showed swelling ratios ranging from 200% to 280%. In deionized (DI) water, the equilibrium swelling ratio for 3D printed hydrogel G5H25 was ~180%, whereas the bulk polymerized hydrogel reached up to ~880%. The cuttlebone-like microstructure induced restrictions on hydrogel swelling which can also be observed in hydrogel G10H20, albeit with a higher swelling ratio likely due to increased Gelatin content. Both 3D printed and bulk polymerized hydrogels of G10H20 displayed increased swelling ratios in PBS buffer solutions, with the 3D printed showing slightly lower swelling (180-200%) compared to the bulk polymerized one (~200-220%) (Figure S7). In DI water, the equilibrium swelling ratio for 3D printed and bulk polymerized hydrogel G10H20

was ~520% and 960%, respectively (Figure S7b). These results indicate that 3D printed hydrogels with cuttlebone-like microstructures can maintain their mechanical properties and dimensional stability in PBS buffer solutions, making them promising candidates for biomedical applications such as scaffolds and tissue engineering.

Cell Adhesion and Biocompatibility. The potential of 3D printed hydrogels for biological applications was next evaluated by measuring their swelling properties and mechanical performance when exposed to full culture media (DMEM high glucose with 10% fetal bovine serum and 1% penicillin/streptomycin). The results, as illustrated in Figure 4a, demonstrate that the swelling ratio of the 3D printed hydrogels was significantly lower than that of their bulk counterparts. Additionally, the stability of the hydrogels was monitored over a 10-day incubation period to determine any effects of degradation under cell culture conditions. Figure 4b shows that hydrogels prepared by bulk polymerization experienced a significant decrease in mechanical integrity over the 10-day incubation period, accompanied by an increase in swelling ratio, indicating that the absorption of solution leads to swelling of the hydrogel and a loss of mechanical strength over time. On the other hand, the loss of mechanical integrity in 3D printed poly(GelMA-*co*-HEMA) hydrogels occurred at a slower rate, with at least 80% of their original rigidity (elastic modulus) being preserved by the end of the 10-day incubation. Surprisingly, the 3D printed G5H25 hydrogel (G5H25-3D) demonstrated an improvement in mechanical properties, with its elastic modulus and tensile strength increasing by 50% over the incubation period (Figure 4b, Figure S8 and Figure S9) which might be attributed to the much lower swelling ratio and additional cross-linkage from the proteins in the cell culture media. The printed cell culture scaffold from G5H25 showed enough hardness and toughness over the 10-day incubation, hence it was used for the following cell culture study. However, hydrogel scaffold made from G5H25 by bulk polymerization collapsed in the cell culture media in less than one day of incubation. This

was attributed to the inherent low elastic modulus of G5H25-B due to the low GelMA content and the swelling-weakening behavior as most reported hydrogels. Therefore, hydrogel G5H25 was unable to be fabricated for subsequent cell culture experiments. To assess the mechanical properties of 3D printed and bulk polymerized scaffolds at cell-relevant length scales that are important in mechanosensing of the matrix. Thus, we measured scaffolds incubated in cell culture media via nanoindentation. While the elastic modulus values obtained via nanoindentation differed from bulk material testing, the trends were consistent among formulations (Figure 4b), in which higher gelatin ratios resulted in stiffer matrices, as well as 3D printing exhibiting greater mechanical strength than bulk polymerized. This suggests that mechanical performance and stability are consistent across length scales and thus useful in a variety of applications.

To identify differences in hardness and toughness changes of hydrogels fabricated by different methods, hydrogel (G10H20) rings (D = 20 mm, H = 10 mm, wall thickness = 5 mm) were prepared by bulk polymerization in a mold or printed on a 3D printer. Figure 4d shows the supporting capability of the hydrogels changing with incubation time. Clearly, hydrogel G10H20 prepared by using the 3D printing method maintained structural stability after loading of 500 g without any noticeable deformation during the 10-day incubation in cell culture media (Figure 4d). However, large deformation can be seen for the bulk polymerized hydrogels after 5 days of incubation. These exciting results suggest that hydrogels with uniform porous structures and thicker polymerized walls achieved by the 3D printing process can significantly enhance the mechanical stability of hydrogels in aqueous media, thereby promoting more applications of such hydrogels in practical bioengineering applications.

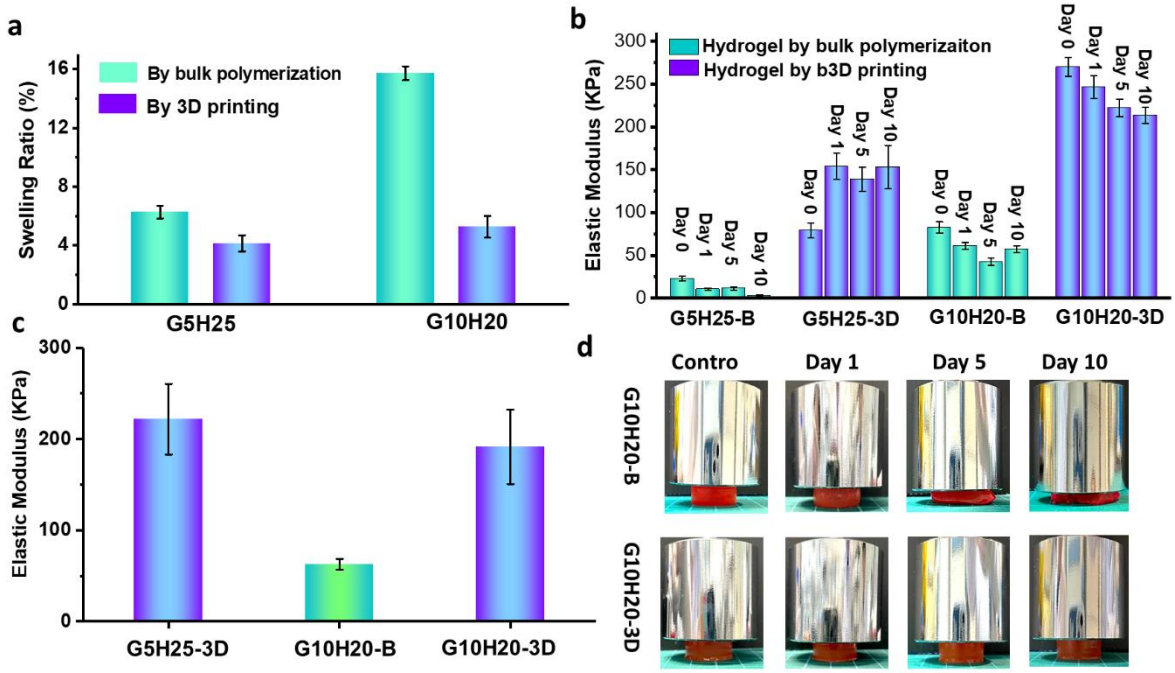

Figure 4. Comparison of (a) percentage swelling ratio and (b) Young's modulus of G5H25 and G10H20 hydrogels fabricated through 3D printing and bulk polymerization when exposed to the cell culture media. (c) Nanoindentation test of the scaffolds used for the cell cultures. (d) Visual representation of compression testing using a 500g standard weight on the as-prepared G10H20-B and G10H20-3D hydrogels and after the hydrogel exposed to cell culture media over day 1, 5 and 10.

To evaluate cellular adhesion and proliferation on bulk polymerized vs. 3D printed grid-shaped hydrogel scaffolds, human dermal fibroblasts cells (WS1) were cultured on G5H25-3D, G10H20-B, and G10H20-3D samples and quantified using a CCK8 assay at days 1, 5, and 10 (Figure 5a). WS1 cells cultured on each hydrogel sample displayed similar attachment and proliferation characteristics after the first 5 days of incubation, with absorbance values at 450nm showing insignificant differences over that period. However, longer incubation periods revealed stark differences between the 3D printed and bulk polymerized hydrogels, with robust proliferation demonstrated only in the 3D printed hydrogel scaffolds. Comparisons among them revealed the highest absorbance in G10H20-3D, followed by G5H25-3D. This indicates that 3D printed hydrogels are more favorable for cell proliferation due to their ability to retain stiffness/rigidity over an extended period.

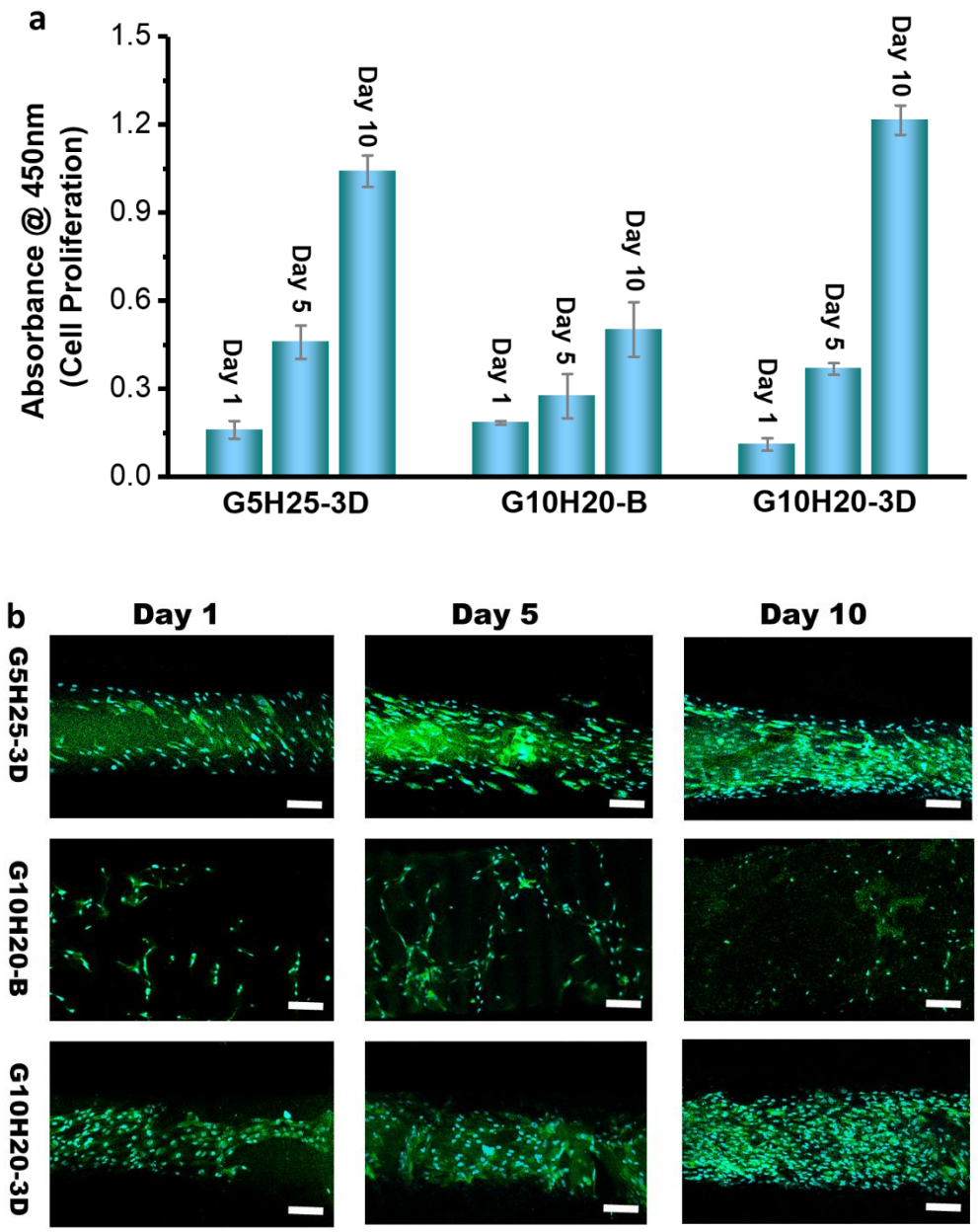

Figure 5. (a) Cell proliferation of WS1 cells cultured on G5H25-3D, G10H20-B and G10H20-3D hydrogels over day 1, 5 and 10. (b) CLSM images of WS1 cell on hydrogel scaffold of G5H25-3D, G10H20-B and G10H20-3D at day 1, 5 and 10 of cultivation after being dyed with Hoechst 33342 and CellMask Green. Blue fluorescence represents cell nucleus; green fluorescence represents cellular plasma membrane. Scale bar: 100 μm.

In addition, confocal microscopy was used to observe cell adhesion and morphological characteristics after labelling the cell nuclei and plasma membrane with Hoechst 33342 and CellMask Green dyes, respectively (Figure 5b). Similar to the cell proliferation results, WS1 cells displayed elongated morphology and favorable attachment to all hydrogel scaffolds on

day 1. However, by day 5, noticeable differences in adherence were observed between the 3D printed and bulk polymerized hydrogels, with G10H20-B having sparse cell attachment, indicating unsuitable mechanical properties that ultimately lead to poor cellular growth. By day 10, minimal cells were present on the hydrogel surface, and those attached had a circular morphology indicating a possibility of imminent cell death. In contrast, cells on G5H25-3D and G10H20-3D hydrogels were well attached and proliferated over the 10 days, suggesting that these hydrogels can provide a favorable microenvironment for the growth and proliferation of WS1 cells.

Conclusions

In summary, we have developed a new approach for significantly enhancing the mechanical properties and stability of poly(GelMA-*co*-HEMA) hydrogels in aqueous media through 3D printing-assisted molecular assembly, resulting in the formation of cuttlebone-like microstructures. Our results show that the bioinspired microarchitecture achieved via 3D printing-assisted polymerization-induced phase separation in the confined space yields a fourfold increase in elastic modulus and exceptional resistance to swelling compared to hydrogels synthesized via bulk polymerization. Furthermore, our study illustrates that 3D printed poly(GelMA-*co*-HEMA) hydrogels exhibit markedly improved mechanical and dimensional stability when subjected to cell culture media, contrasting with conventional bulk-polymerized hydrogels, which often experience collapse, deformation, and loss of mechanical strength under similar conditions. The bioinspired strategy presented here demonstrates an approach to restrict hydrogel swelling while providing enhanced mechanical stability, addressing the long-term challenges in utilizing hydrogels for bioengineering applications.

Methods and Material

Synthesis of Methacrylated Gelatin (GelMA). Gelatin methacryloyl was synthesized by modification of our previous report procedure.[63] In brief, 100 gram of type A bovine skin gelatin (300 bloom, Sigma Aldrich) was dissolved into 800 ml of 0.25 M carbonate buffer solution at 50 °C. Then, 10 mL of methacrylic anhydride (MA) was added dropwise at 4 mL/hour under magnetic stirring at 400 rpm at temperate of 50 °C. After 3 hours reaction, the reaction mixture was left overnight at 37 °C and then neutralized to pH = 7 with hydrochloride acid. The solution was filtered and dialyzed in a MWCO 12,000-14,000 dialysis tubing (Sigma Aldrich) against DI water for 1 week at room temperature, and subsequently lyophilized to yield a white powder. The Degree of methylacrylation (DM) of GelMA was determined by ^{1}H NMR spectra(JEOL ECA500II spectrometer) operating at frequency of 400 MHz (Figure S10). Gelatin and dried GelMA powder were dissolved in D_2O to a concentration of ~30 mg/mL at 40 °C till a homogeneous solution was obtained. The DM of GelMA was defined as the number of methacrylate groups per available lysine found in the gelatin and was determined by ^{1}H NMR in D_2O according to the reference.[64] The DM of GelMA in the present work was found to be approximately 87 %.

Preparation of GelMA: HEMA Printing Ink. Solution preparation was conducted by dissolving various concentrations (5 wt%, 10 wt%) of GelMA powder into 70 wt% of DI water at 50 °C till a homogenous solution was obtained. Subsequently, HEMA of various concentrations (20 wt%, 25 wt%) and 0.5 wt% of LAP were added into the solution and sonicated until all constituents were dispersed uniformly.

Preparation of Bulk Polymerized poly(GelMA-*co*-HEMA) Hydrogels. Bulk polymerized hydrogel samples were prepared though UV exposure of hydrogel solution placed between a glass mold. Briefly, 50mL of hydrogel solution was poured between a 100 mm × 35 mm × 1.6 mm glass mold and placed in a UV cross linker chamber (405nm) for 5 minutes for

polymerization to occur. Samples were gently removed from the mold, cut to size with a razor cutter and kept in a 4 °C fridge till required.

3D Printing of the poly(GelMA-*co*-HEMA) Hydrogels. 3D printed hydrogel samples were fabricated using Anycubic Photon 3D printer (λ = 405 nm, Shenzhen Anycubic Technology Co., Ltd., China) with layer thickness of 0.05 mm and normal exposure time varied between 20 to 65 seconds depending on each respective solution's curing time (the specific printing conditions are provided in Table S1). After printing, the samples were post-cured in the UV cross linker chamber(λ = 405 nm) for 5 minutes, cut to size using a razer cutter and kept in a 4 °C fridge till required.

Mechanical Analysis. To measure the Young's modulus, ultimate tensile stress and maximum strain, mechanical tests were performed with at least 5 replicates on a Instron 5569 (Instron Corporation, MA, USA) equipped with a non-contact video extensometer at a ramp rate of 20mm/min using a 100-N load cell. Both as-prepared bulk and 3D printed hydrogels together with those exposed to cell culture medium over 1 day, 5 days and 10 days were subjected to testing. The tensile strength of hydrogels was calculated by dividing the maximum load with the original cross-sectional area of the test specimen. The young's modulus of hydrogels was calculated as the slope of the linear portion of the stress–strain curve. Nanoindentation of the scaffolds were conducted after soaking in cell media for 4 hours. In all nanoindentation tests, at least 3 replicates were conducted for each scaffold, with 10 indentation readings taken on each replicate. The readings were averaged to determine the mean elastic modulus values for statistical purposes.

Water Content Analysis. The water content of hydrogels were determined gravimetrically by measuring of wet weight (W_w) and dried weight (W_d) of the as-prepared hydrogels. The wet weight (W_w) was measured after removing the surface moisture of the hydrogel by wiping it with paper. After drying the hydrogel in a 45 °C oven for 24 hours, the dried weight

(W_d) was measured, and the water content of hydrogels was calculated from the following equation: Water content (%) = $(W_w\text{-}W_d)/W_w \times 100$. Measurements were performed 3 times for each sample and the results were displayed as a mean ± standard deviation.

Swelling and Shrinking Kinetics. Both bulky polymerized and 3D printed hydrogel samples were cut into 1cm diameter circles with a thickness of 1.6 mm and freeze-dried overnight. After initial weighing (W_0), the specimens were incubated in different solutions include cell culture media, Phosphate Buffer Saline (PBS) of various pH values (5.4, 6.5, 7.4, 10) and DI water. The incubated samples were taken out to measure the real time weight of hydrogel (W_t) at various time intervals (10, 20 30, 60, 90, 300mins). The swelling ratio of the hydrogels was defined using the following equation:[65]

Swelling ratio (%) = $(W_t\text{-}W_o)/W_o \times 100$

Microstructure Morphology Analysis. The cross-sectional areas of both bulk and 3D printed hydrogel samples were analyzed using a Field-emission scanning electron microscope (FE-SEM, HITACHI FESEM SU8220) operated at 5 kV. Prior to SEM analysis, 1 cm^2 samples were immersed in DI water for a short period of time, freeze-dried (Martin Christ) overnight and coated with a thin graphite layer. Post-processing was conducted using ImageJ software (National Institutes of Health, Bethesda, USA).

3D Printing of poly(GelMA-*co*-HEMA) Grid Structure for Cellular Growth. A grid STL file was extracted from the freecad database and modified with minor changes for 3D printing. Hydrogel samples were prepared in a sterile environment using similar formulations described previously and the honeycomb structure was printed using the same printing parameters as before.

WS1 Cell Culture and Seeding on poly(GelMA-*co*-HEMA) Hydrogels. Human dermal fibroblasts (WS1) gotten from ATCC were maintained in DMEM medium supplemented

with 10% Fetal Bovine Serum and 1% Penicillin / Streptomycin till 80% confluent. Prior to cell seeding, hydrogel samples were UV sterilized for 30 minutes, washed and pre-incubated with cell media overnight. Aliquots of the cell suspension were seeded on the grid scaffolds to achieve an initial cell density of 1×10^5 cells/cm^2. The cell-seeded hydrogels were incubated for 4 hours to ensure attachment of cells. Thereafter, unbound cells were washed off, fresh media was topped up and the cell-laden hydrogels were left for 1 day, 5 days and 10 days before further tests were conducted. Cell media was refreshed every 2 days.

Compression Analysis. A cylindrical STL file with dimensions of 20 mm diameter with 5 mm hollow radius and 10 mm in height was designed in Free CAD. Selected samples were polymerized or 3D printed using a similar method as mentioned above. Thereafter, samples were sterilized, placed in a 12-well plate and soaked in complete cell culture media in the incubator at 37 °C, 5% CO_2. After days 1, 5 and 10 respectively, samples were removed and compressed using a 500 g standard weight for 15 seconds. Images were captured using an Iphone 13.

WS1 Cell Attachment and Proliferation. WS1 adhesion and proliferation capability towards poly(GelMA-*co*-HEMA) grid scaffolds were assessed using Cell-Counting Kit-8(CCK8) reagent. After incubation periods of 1 day, 5 days and 10 days, the cell-laden scaffolds were washed thrice with 1x sterile PBS before 10% CCK-8 solution mixed with cell media was added into each well. Optical density at 450 nm was measured using a multifunction microplate reader (Infinite M200 Pro, Tecan) after incubation for 2 h at 37 °C.

Fluorescence Cell Imaging. Cellular growth and morphology were qualitatively analyzed using fluorescence imaging of its nucleus and cell membrane. Hoechst 33342 cell staining solution was prepared by either diluting the Hoechst 33342 stock solution 1 : 2,000 in 1× PBS or CellMask Green cell-labeling solution 1:1,000 in complete cell media. Prior to staining, after day 1, 5 and 10 of incubation, cells were fixed with 4 % (w/v)

paraformaldehyde at room temperature for 15 min. Sufficient Hoechst 33342 staining solution was added and incubated for 5–10 minutes away from light. Thereafter, the Hoechst 33342 staining solution was decanted and hydrogel scaffolds were washed three times with 1× PBS to remove unbound dye. Next, CellMask Green staining solution was added to the scaffolds and incubated at 37 °C for 15 minutes. Thereafter, the staining solution was decanted and samples were washed five times with warm cell media to remove unbound dye. Samples were imaged using a Confocal Laser Scanning Microscope (Leica, Germany).

Supporting Information

The Supporting Information is available free of charge at https://pubs.acs.org/.

Pore size distribution, comparison of the programmed printing layer height and measured samples layer thickness, Optical microscope images of the 3D printed wet hydrogels, SEM images of cross-sectional for hydrogels, comparison of the transparency of hydrogels, water content and gel fraction percentages, swelling ratio of hydrogel, photos of hydrogel after incubation, tensile curves, comparative NMR spectra of Gelatin and synthesized Gelatin-MA and detailed printing conditions for different composition and leyer-thickness.

Acknowledgement

This work was supported by SERC Central Research Fund (TIMR211001bSERCRF) and the MTC Individual Research Grants (M23M6c0110) from A*STAR of Singapore. The biocompatibility study was supported by the Ministry of Education under the Research Centres of Excellence programme through the Mechanobiology Institute at the National University of Singapore and the Biomedical Engineering Department at the National University of Singapore.

Author contributions

HLC and FKW conceived the printing strategy and materials assembly design. FKW prepared and revised the paper. HLC, YM, JK, JWK developed the materials and printed, and tested physical properties of the samples. CHL did the cell culture and data collection, FHR and JLY worked on scaffold nanoindentation and LP measured the SEM images of the samples.

Conflict of Interest

The authors declare no conflict of interest.

Data Availability Statement

The data that support the findings of this study are available from the corresponding author upon reasonable request.

References

(1) Karimi, F.; O'Connor, A. J.; Qiao, G. G.; Heath, D. E. Integrin clustering matters: a review of biomaterials functionalized with multivalent integrin‐binding ligands to improve cell adhesion, migration, differentiation, angiogenesis, and biomedical device integration. *Advanced healthcare materials* **2018**, *7* (12), 1701324.
(2) Kiradzhiyska, D. D.; Mantcheva, R. D. Overview of biocompatible materials and their use in medicine. *Folia Med (Plovdiv)* **2019**, *61* (1), 34-40.
(3) Yue, S.; He, H.; Li, B.; Hou, T. Hydrogel as a biomaterial for bone tissue engineering: A review. *Nanomaterials* **2020**, *10* (8), 1511.
(4) Cao, H.; Duan, L.; Zhang, Y.; Cao, J.; Zhang, K. Current hydrogel advances in physicochemical and biological response-driven biomedical application diversity. *Signal transduction and targeted therapy* **2021**, *6* (1), 426.
(5) Li, M.; Lv, J.; Yang, Y.; Cheng, G.; Guo, S.; Liu, C.; Ding, Y. Advances of Hydrogel Therapy in Periodontal Regeneration—A Materials Perspective Review. *Gels* **2022**, *8* (10), 624.
(6) Rosales, A. M.; Anseth, K. S. The design of reversible hydrogels to capture extracellular matrix dynamics. *Nature Reviews Materials* **2016**, *1* (2), 1-15.
(7) Feng, W.; Wang, Z. Tailoring the Swelling‐Shrinkable Behavior of Hydrogels for Biomedical Applications. *Advanced Science* **2023**, *10* (28), 2303326.
(8) Kamata, H.; Akagi, Y.; Kayasuga-Kariya, Y.; Chung, U.-i.; Sakai, T. "Nonswellable" hydrogel without mechanical hysteresis. *Science* **2014**, *343* (6173), 873-875.
(9) Kamata, H.; Kushiro, K.; Takai, M.; Chung, U. i.; Sakai, T. Non‐osmotic hydrogels: a rational strategy for safely degradable hydrogels. *Angewandte Chemie International Edition* **2016**, *55* (32), 9282-9286.
(10) Bian, S.; Hao, L.; Qiu, X.; Wu, J.; Chang, H.; Kuang, G. M.; Zhang, S.; Hu, X.; Dai, Y.; Zhou, Z. An injectable rapid‐adhesion and anti‐swelling adhesive hydrogel for hemostasis and wound sealing. *Advanced Functional Materials* **2022**, *32* (46), 2207741.
(11) Wu, J.; Pan, Z.; Zhao, Z. Y.; Wang, M. H.; Dong, L.; Gao, H. L.; Liu, C. Y.; Zhou, P.; Chen, L.; Shi, C. J. Anti‐Swelling, Robust, and Adhesive Extracellular Matrix‐Mimicking Hydrogel Used as Intraoral Dressing. *Advanced Materials* **2022**, *34* (20), 2200115.

(12) Park, J.; Kim, J. Y.; Heo, J. H.; Kim, Y.; Kim, S. A.; Park, K.; Lee, Y.; Jin, Y.; Shin, S. R.; Kim, D. W. Intrinsically Nonswellable Multifunctional Hydrogel with Dynamic Nanoconfinement Networks for Robust Tissue‐Adaptable Bioelectronics. *Advanced Science* **2023**, *10* (12), 2207237.
(13) Di, X.; Hou, J.; Yang, M.; Wu, G.; Sun, P. A bio-inspired, ultra-tough, high-sensitivity, and anti-swelling conductive hydrogel strain sensor for motion detection and information transmission. *Materials Horizons* **2022**, *9* (12), 3057-3069.
(14) Delplace, V.; Nickerson, P.; Ortin-Martinez, A.; Baker, A. EG; Wallace, VA; Shoichet, MS Nonswelling, Ultralow Content Inverse Electron-Demand Diels-Alder Hyaluronan Hydrogels with Tunable Gelation Time: Synthesis and In Vitro Evaluation. *Adv. Funct. Mater* **2020**, *30* (14), 1903978.
(15) Zhang, J.; Yong, H.; Xu, Q.; Miao, Y.; Lyu, J.; Gao, Y.; Zeng, M.; Zhou, D.; Yu, Z.; Tai, H. Structural design of robust and biocompatible photonic hydrogels from an in situ cross-linked hyperbranched polymer system. *Chemistry of Materials* **2018**, *30* (17), 6091-6098.
(16) Luo, C.; Huang, M.; Sun, X.; Wei, N.; Shi, H.; Li, H.; Lin, M.; Sun, J. Super-strong, nonswellable, and biocompatible hydrogels inspired by human tendons. *ACS Applied Materials & Interfaces* **2022**, *14* (2), 2638-2649.
(17) Bertsch, P.; Diba, M.; Mooney, D. J.; Leeuwenburgh, S. C. Self-healing injectable hydrogels for tissue regeneration. *Chemical Reviews* **2022**, *123* (2), 834-873.
(18) Kirillova, A.; Yeazel, T. R.; Asheghali, D.; Petersen, S. R.; Dort, S.; Gall, K.; Becker, M. L. Fabrication of biomedical scaffolds using biodegradable polymers. *Chemical reviews* **2021**, *121* (18), 11238-11304.
(19) Qi, C.; Dong, Z.; Huang, Y.; Xu, J.; Lei, C. Tough, anti-swelling supramolecular hydrogels mediated by surfactant–polymer interactions for underwater sensors. *ACS Applied Materials & Interfaces* **2022**, *14* (26), 30385-30397.
(20) De Serres-Berard, T.; Becher, T. B.; Braga, C. B.; Ornelas, C.; Berthod, F. Neuropeptide Substance P released from a nonswellable laponite-based hydrogel enhances wound healing in a tissue-engineered skin in vitro. *ACS Applied Polymer Materials* **2020**, *2* (12), 5790-5797.
(21) Pi, M.; Qin, S.; Wen, S.; Wang, Z.; Wang, X.; Li, M.; Lu, H.; Meng, Q.; Cui, W.; Ran, R. Rapid Gelation of Tough and Anti‐Swelling Hydrogels under Mild Conditions for Underwater Communication. *Advanced Functional Materials* **2023**, *33* (1), 2210188.
(22) Wang, S.; Zhang, D.; He, X.; Zhou, J.; Zhou, Y.; Wang, X.; Wang, Z.; Liu, S.; Zheng, S. Y.; Yang, J. Anti-Swelling Zwitterionic Hydrogels as Multi-Modal Underwater Sensors and All-in-One Supercapacitors. *ACS Applied Polymer Materials* **2022**, *4* (10), 7498-7507.
(23) Xu, P.; Wang, L.; Zhang, X.; Yan, J.; Liu, W. High-performance smart hydrogels with redox-responsive properties inspired by scallop byssus. *ACS Applied Materials & Interfaces* **2021**, *14* (1), 214-224.
(24) Kim, Y.-W.; Kim, J. E.; Jung, Y.; Sun, J.-Y. Non-swellable, cytocompatible pHEMA-alginate hydrogels with high stiffness and toughness. *Materials Science and Engineering: C* **2019**, *95*, 86-94.
(25) Dou, X.; Wang, H.; Yang, F.; Shen, H.; Wang, X.; Wu, D. One‐Step Soaking Strategy toward Anti‐Swelling Hydrogels with a Stiff “Armor”. *Advanced Science* **2023**, *10* (9), 2206242.
(26) Liu, J.; Chen, Z.; Chen, Y.; Rehman, H. U.; Guo, Y.; Li, H.; Liu, H. Ionic conductive organohydrogels with dynamic pattern behavior and multi‐environmental stability. *Advanced Functional Materials* **2021**, *31* (24), 2101464.
(27) Liu, X.; Zhang, Q.; Gao, G. DNA-inspired anti-freezing wet-adhesion and tough hydrogel for sweaty skin sensor. *Chemical Engineering Journal* **2020**, *394*, 124898.
(28) Liu, X.; Zhang, Q.; Duan, L.; Gao, G. Bioinspired nucleobase-driven nonswellable adhesive and tough gel with excellent underwater adhesion. *ACS applied materials & interfaces* **2019**, *11* (6), 6644-6651.
(29) Liu, Y.; Liu, J.; Chen, S.; Lei, T.; Kim, Y.; Niu, S.; Wang, H.; Wang, X.; Foudeh, A. M.; Tok, J. B.-H. Soft and elastic hydrogel-based microelectronics for localized low-voltage neuromodulation. *Nature biomedical engineering* **2019**, *3* (1), 58-68.
(30) Taboada, G. M.; Yang, K.; Pereira, M. J.; Liu, S. S.; Hu, Y.; Karp, J. M.; Artzi, N.; Lee, Y. Overcoming the translational barriers of tissue adhesives. *Nature Reviews Materials* **2020**, *5* (4), 310-329.

(31) Yang, Y.; Song, X.; Li, X.; Chen, Z.; Zhou, C.; Zhou, Q.; Chen, Y. Recent progress in biomimetic additive manufacturing technology: from materials to functional structures. *Advanced Materials* **2018**, *30* (36), 1706539.
(32) Wang, B.; Sullivan, T. N.; Pissarenko, A.; Zaheri, A.; Espinosa, H. D.; Meyers, M. A. Lessons from the ocean: whale baleen fracture resistance. *Advanced Materials* **2019**, *31* (3), 1804574.
(33) Ortiz, C.; Boyce, M. C. Bioinspired structural materials. *Science* **2008**, *319* (5866), 1053-1054.
(34) Liu, C.; Ji, X.; Huang, J.; Wang, Z.; Liu, Y.; Hincke, M. T. Proteomics of shell matrix proteins from the cuttlefish bone reveals unique evolution for cephalopod biomineralization. *ACS Biomaterials Science & Engineering* **2021**.
(35) Yang, T.; Jia, Z.; Chen, H.; Deng, Z.; Liu, W.; Chen, L.; Li, L. Mechanical design of the highly porous cuttlebone: A bioceramic hard buoyancy tank for cuttlefish. *Proceedings of the National Academy of Sciences* **2020**, *117* (38), 23450-23459.
(36) Ren, K.-f.; Hu, M.; Zhang, H.; Li, B.-c.; Lei, W.-x.; Chen, J.-y.; Chang, H.; Wang, L.-m.; Ji, J. Layer-by-layer assembly as a robust method to construct extracellular matrix mimic surfaces to modulate cell behavior. *Progress in Polymer Science* **2019**, *92*, 1-34.
(37) Finnemore, A.; Cunha, P.; Shean, T.; Vignolini, S.; Guldin, S.; Oyen, M.; Steiner, U. Biomimetic layer-by-layer assembly of artificial nacre. *Nature communications* **2012**, *3* (1), 966.
(38) Tang, Z.; Wang, Y.; Podsiadlo, P.; Kotov, N. A. Biomedical applications of layer‐by‐layer assembly: from biomimetics to tissue engineering. *Advanced materials* **2006**, *18* (24), 3203-3224.
(39) Wang, Z.; Heck, M.; Yang, W.; Wilhelm, M.; Levkin, P. A. Tough PEGgels by in situ phase separation for 4D printing. *Advanced Functional Materials* **2024**, *34* (20), 2300947.
(40) Brosch, S.; Belardo, S.; Mertens, A.-K.; Linkhorst, J.; Wessling, M. In Situ Visualization of Polymerization-Induced Phase Separation for 3D-Printing of Porous Architectures. *Macromolecules* **2024**, *57* (3), 1220-1228.
(41) Li, P.; Dou, X.; Feng, C.; Schönherr, H. Enhanced cell adhesion on a bio-inspired hierarchically structured polyester modified with gelatin-methacrylate. *Biomaterials science* **2018**, *6* (4), 785-792.
(42) Kim, A. Y.; Kim, Y.; Lee, S. H.; Yoon, Y.; Kim, W.-H.; Kweon, O.-K. Effect of gelatin on osteogenic cell sheet formation using canine adipose-derived mesenchymal stem cells. *Cell Transplantation* **2017**, *26* (1), 115-123.
(43) Samavedi, S.; Poindexter, L. K.; Van Dyke, M.; Goldstein, A. S. Synthetic biomaterials for regenerative medicine applications. In *Regenerative medicine applications in organ transplantation*, Elsevier, 2014; pp 81-99.
(44) Li, J.; Chee, H. L.; Chong, Y. T.; Chan, B. Q. Y.; Xue, K.; Lim, P. C.; Loh, X. J.; Wang, F. Hofmeister effect mediated strong PHEMA-gelatin hydrogel actuator. *ACS Applied Materials & Interfaces* **2022**, *14* (20), 23826-23838.
(45) Kilic Bektas, C.; Hasirci, V. Cell Loaded GelMA: HEMA IPN hydrogels for corneal stroma engineering. *Journal of Materials Science: Materials in Medicine* **2020**, *31*, 1-15.
(46) Weaver, J.; Bannister, I.; Robinson, K.; Bories-Azeau, X.; Armes, S.; Smallridge, M.; McKenna, P. Stimulus-responsive water-soluble polymers based on 2-hydroxyethyl methacrylate. *Macromolecules* **2004**, *37* (7), 2395-2403.
(47) Guan, F.; Yang, L.; Wang, J.; Guan, B.; Han, K.; Wang, Q.; Zhu, L. Confined ferroelectric properties in poly (vinylidene fluoride‐co‐chlorotrifluoroethylene)‐graft‐polystyrene graft copolymers for electric energy storage applications. *Advanced Functional Materials* **2011**, *21* (16), 3176-3188.
(48) Fan, Y.; Wu, K.-T.; Aghvami, S. A.; Fraden, S.; Breuer, K. S. Effects of confinement on the dynamics and correlation scales in kinesin-microtubule active fluids. *Physical Review E* **2021**, *104* (3), 034601.
(49) Essafri, I.; Morineau, D.; Ghoufi, A. Microphase separation of a miscible binary liquid mixture under confinement at the nanoscale. *Npj Computational Materials* **2019**, *5* (1), 42.
(50) Dušek, K.; Sedláček, B. Phase separation in poly (2-hydroxyethyl methacrylate) gels in the presence of water. *European Polymer Journal* **1971**, *7* (9), 1275-1285.
(51) Lou, X.; Munro, S.; Wang, S. Drug release characteristics of phase separation pHEMA sponge materials. *Biomaterials* **2004**, *25* (20), 5071-5080.

(52) Liu, Q.; Hedberg, E. L.; Liu, Z.; Bahulekar, R.; Meszlenyi, R. K.; Mikos, A. G. Preparation of macroporous poly (2-hydroxyethyl methacrylate) hydrogels by enhanced phase separation. *Biomaterials* **2000**, *21* (21), 2163-2169.
(53) Zare, M.; Bigham, A.; Zare, M.; Luo, H.; Rezvani Ghomi, E.; Ramakrishna, S. pHEMA: An overview for biomedical applications. *International Journal of Molecular Sciences* **2021**, *22* (12), 6376.
(54) Das, D.; Pal, S. Dextrin/poly (HEMA): pH responsive porous hydrogel for controlled release of ciprofloxacin. *International journal of biological macromolecules* **2015**, *72*, 171-178.
(55) Chen, F.; Li, X.; Yu, Y.; Li, Q.; Lin, H.; Xu, L.; Shum, H. C. Phase-separation facilitated one-step fabrication of multiscale heterogeneous two-aqueous-phase gel. *Nature Communications* **2023**, *14* (1), 2793.
(56) Mace, C. R.; Akbulut, O.; Kumar, A. A.; Shapiro, N. D.; Derda, R.; Patton, M. R.; Whitesides, G. M. Aqueous multiphase systems of polymers and surfactants provide self-assembling step-gradients in density. *Journal of the American Chemical Society* **2012**, *134* (22), 9094-9097.
(57) Rouf, S.; Raina, A.; Haq, M. I. U.; Naveed, N.; Jeganmohan, S.; Kichloo, A. F. 3D printed parts and mechanical properties: influencing parameters, sustainability aspects, global market scenario, challenges and applications. *Advanced Industrial and Engineering Polymer Research* **2022**.
(58) Wang, X.; Song, X.; Tang, W.; Zhao, S.; Xu, X. Microstructure Effects on Mechanical Properties of Network-Forming Polymer Systems: An Atomistic Simulation Study. *Chemical Engineering Science* **2023**, 118986.
(59) Lee, E.; Jia, Z.; Yang, T.; Li, L. Multiscale mechanical design of the lightweight, stiff, and damage-tolerant cuttlebone: A computational study. *Acta Biomaterialia* **2022**, *154*, 312-323.
(60) Mao, A.; Zhao, N.; Liang, Y.; Bai, H. Mechanically efficient cellular materials inspired by cuttlebone. *Advanced Materials* **2021**, *33* (15), 2007348.
(61) Zhang, X.; Guo, A.; Ma, X.; Du, H.; Yan, L.; Hou, F.; Liu, J. Cuttlefish-Bone-Structure-like Lamellar Porous Fiber-Based Ceramics with Enhanced Mechanical Performances. *ACS Applied Materials & Interfaces* **2023**, *15* (10), 13121-13130.
(62) Yan, X.; Bethers, B.; Chen, H.; Xiao, S.; Lin, S.; Tran, B.; Jiang, L.; Yang, Y. Recent advancements in biomimetic 3d printing materials with enhanced mechanical properties. *Frontiers in Materials* **2021**, *8*, 518886.
(63) Chee, H. L.; Koo, J. W.; Sim, E. E. I.; Zhu, Q.; Gao, X.; Ramli, M. F. H.; Young, J. L.; Holle, A. W.; Wang, F. Hofmeister Ions‐Induced Thinning of Gelatin to Enhance 3D Printing Precision. *Advanced Materials Technologies*, 2302230.
(64) Hoch, E.; Schuh, C.; Hirth, T.; Tovar, G. E.; Borchers, K. Stiff gelatin hydrogels can be photo-chemically synthesized from low viscous gelatin solutions using molecularly functionalized gelatin with a high degree of methacrylation. *Journal of Materials Science: Materials in Medicine* **2012**, *23*, 2607-2617.
(65) Zhao, X.; Lang, Q.; Yildirimer, L.; Lin, Z. Y.; Cui, W.; Annabi, N.; Ng, K. W.; Dokmeci, M. R.; Ghaemmaghami, A. M.; Khademhosseini, A. Photocrosslinkable gelatin hydrogel for epidermal tissue engineering. *Advanced healthcare materials* **2016**, *5* (1), 108-118.

Table Of Contents